Supporting Information

A Highly Selective Gas Sensor Based on Hydrophobic Silica Decorated with Trimethoxyoctadecylsilane

Juan Xie*, Lei Zhang, Biao Liu, Penghui Bai, Chenjie Wang, Jiake Xu, and Hu Wang*

School of New Energy and Materials, Southwest Petroleum University (SWPU), Chengdu 610500, China

*Corresponding author.

Tel.: +86 28 83037480;

Fax: +86 28 83037480;

E-mail address: jxie@swpu.edu.cn (J. Xie); hwang@swpu.edu.cn (H. Wang).

CONTENTS

Chapter 1. Reviews

As for mesoporous silica, shown great potential for sensing applications, which has been widely researched. B.J. Melde[1] and J.E. Amonette[2] proposed reviews about mesoporous silica and silica aerogels materials in sensing. In order to improve the particular sensing performance of silica, modification of silica such as microstructure synthesis, surface functionalization and composites were deeply studied, which we concluded as Table S1.[3-22,42] Besides, the alkyl decorated silica materials were also widely researched, which were applied in multiple fields (shown as Table S2).[23-38] Z.K. Wang et al. fabricated the hexadecyl decorated silica by chemical co-immobilization method, which could selectively adsorb bisphenol A from aqueous solution. M.S. Milla et al.[27] successfully synthesized ammonium alkyl chains decorated silica, which exhibited excellent antibacterial property. D.N. Huang et al.[37] prepared octadecyltriethoxysilane decorated silica by three-steps method, which could efficiently enrich the phthalates. There were few reports about the trimethoxyoctadecylsilane (OTMS) alkyl group, which were applied in superhydrophobic material when decorated with CeO_2,[39] antiwear ability of liquid paraffin when decorated with TiO_2,[40] improving extraction efficiency for nonpolar benzene homologues when decorated with ZnO,[41] seldom did the report about decoration with silica and the application in gas sensing.

Table S1. Summary of modified silica applied in gas sensing.

Materials	Synthesis method	Sensor types	Properties	Ref.
Various microstructures of silica				
Ordered silica spheres	Sol-gel method	QCM	Selectively detected alcohol vapors	3
Hollow silica tube	-	Interferometric gas sensor	Applied for gas-concentration analysis	4
Polymer-clad silica	Sol-gel method	Fiber optic sensor	Chlorinated hydrocarbons can be detected at low limit	5
Silica nanowire	-	Optical gas sensor	Applied for the leakage detection of propane	6
Microporous silica	Slight alteration	Electrochemical sensor	Applied for humidity sensor	7
Silica photonic crystal	Sol-gel method	Optical gas sensor	Applied for gas-sensing with photonic bandgap shift	42
Silica aerogel	Sol-gel method	Electrochemical sensor	Applied for humidity sensor	8

Surface functionalization of silica				
Metallo-porphyrin silica	-	Fiber optic sensor	O_2 sensing for long term use in jet fuel	9
PDA-HMSSs [a]	Adjust the dopamine concentration	QCM	Selectively detected HCHO in food	10
DAP [b]-silica aerogel	Co-gelation process	Optical gas sensor	Applied for O_2 sensing	11
4-BMC [c]-silica aerogel	SCR [d]	Optical gas sensor	Applied for O_2 sensing	12
PtOEP [e]-silica aerogel	-	Optical gas sensor	Applied for O_2 sensing	13
PANI-silica aerogel	Kaner's rapid mixing process	Chemiresistive gas sensor	Applied for HCl and NH_3 sensing	14
MTMS [f]-silica	One-pot method	Optical gas sensor	Applied for TNT sensing	15
Silica composite materials (includes doping, core-shell structure)				
CeO_2/SiO_2	Sol-hydrothermal route	Chemiresistive gas sensor	Enhanced NH_3 gas-sensing	16
C/SiO_2	Template-carbonization strategy	QCM	Showed excellent sensing performances to indoor VOCs	17

$NiO/Au/SiO_2$	Sol-gel method	SAW	Selectively recognized H_2 in the presence of CO	18
$SiO_2 \cdot x$ZrP [g]	Vacuum drying method	Solid state sensor	Detected O_2 at room temperature in a dry environment	19
SiO_2/ZnO core/shell	In a triton X-100 system	Chemiresistive gas sensor	Highly selective to ethanol	20
$Ru(bpy)_3^{2+}$ doped silica	Slight modification	Electrochemiluminescent sensor	Selective detection for H_2S	21
ZnO/silica foam	-	Optical gas sensor	Applied for ethanol gas sensor	22

[a] PDA-HMSSs: poly-dopamine functionalized hollow mesoporous silica spheres. [b] DAP: N-(3-trimethoxysilylpropyl)-2,7-diazapyrenium. [c] 4-BMC: 4-Benzoyl-N-methylpyridinium cation. [d] SCR: sonogashira coupling reaction. [e] PtOEP: platinum octaethylporphine. [f] MTMS: methyltrimethoxysilane. [g] $SiO_2 \cdot x$ZrP: silica-zirconium phosphate-phosphoric acid composites.

Table S2. Summary of application of alkyl decorated silica.

Alkyl groups	Silica microstructures	Synthesis method	Fields of application	Ref.
C1Q [a], C4Q [b], C12Q [c] and C18Q [d]	Mesoporous silica	Surface modification	Selective nitrate removal from aqueous solution	23
Cobalt(II) alkyl phosphonate	Mesoporous MCM-41	-	Selective oxidations of allylic alcohols	24
Vanadyl alkyl phosphonate	Silica	-	Selective oxidation of sulfides to sulfoxides	25
Dodecyl	MCM-41	Hydrothermal synthesis	Molecular selective adsorption from water	26
Hexadecyl	Silica	Chemical co-immobilization	Bisphenol A adsorption from aqueous solution	27
C18 alkyl	Silica gels	Surface coverage	Research on the conformational order of C18	28
C16 [e]	Colloidal silica	-	Research on charging of silica in apolar media	29
Ammonium alkyl chains	Silica	-	Research on the antibacterial properties	30
Short alkyl chains	Silica NPs	Carbodiimide chemistry	Research on the moderate activation	31

C6, C10 and C16 alkyl	Silica	Sol-gel method	Research on the thermal properties	32
C18 [f]	Silica	Surface modification	Research on the improved separation effiency	33
C18 cartridges	Silica	-	Research on the adsorption towards pesticides	34
C18 (unknown)	Silica	-	Research on the adsorption of peptide	35
C18 (unknown)	Silica	-	Rapid detecting metal ions by chromatography	36
C18 [g]	Graphene-silica	Three-steps method	Efficient enrichment of phthalates	37
C18 (OTMS)	Monolayer SiO_2/Si	CVD	Research on the synthesis	38
C18 (OTMS)	Mesoporous silica	Surface modification	Selective gas sensing	This work

[a] C1Q: trimethy[3-(trimethoxysilyl)propyl] ammonium chloride. [b] C4Q: dimethylbuty[3-(trimethoxysilyl)propyl] ammonium chloride. [c] C12Q: dimethyldodecy[3-(trimethoxysilyl)propyl] ammonium chloride. [d] C18Q: dimethyloctadecy[3-(trimethoxysilyl)propyl] ammonium chloride. [e] C16: hexadecyltrimethoxysilane. [f] C18: chlorodimethyloctadecylsilane. [g] C18: octadecyltriethoxysilane.

Chapter 2. Materials and Instrumentation

2.1 Materials.

All chemical reagents and solvents were purchased from Kelong Chemical Reagent Co., Ltd. (Chengdu, China) and used as received without further purification. Deionized (DI) water was obtained from a Milli-Q water purification system. High purity gases (99.9999%) including oxide, nitrogen, argon and carbon dioxide, were obtained from Jinnengda Co., Ltd. (Chengdu, China). Premixed gas tank of hydrogen with the concentration of 5% (95% argon) was purchased from Jinnengda Co., Ltd. (Chengdu, China).

2.2 Instrumentation.

Scanning electron microscopy (SEM) images were collected from a scanning electron microscope (Zeiss EVO MA15) at an acceleration voltage of 10 kV. The size of crystals was calculated from SEM images of different areas of the same sample by using ImageJ software.

Mass Flow Controller (MFC) and syringes were provided by Ristron Co., Ltd (Jiaxing, China). Quartz Crystal Microbalance (QCM) of SRS 200 was purchased from Deshang Co., Ltd. (Tianjin, China).

Fourier transform infrared reflection (FTIR) spectrum (WQF520) was provided by Ruili Co., Ltd (Beijing, China).

Automatic contact angle tester (OCA25) was provided by Dataphysics Instruments GmbH. Contact Angle (CA) was measured by attached software.

Volumetric N_2 sorption measurements were carried out at 77 K by using gas adsorption system (Quantachrome QuadraSorb-SI2000-09). Specific surfaces areas were calculated from the N_2 adsorption data according to the Brunauer-Emmett-Teller (BET) method. Cumulative pore volumes and pore diameters were calculated from the adsorption isotherms by the Barrett-Joyner-Halenda (BJH) method.

Chapter 3. Characterizations

3.1 BET measurement.

Representative N_2 sorption isotherm of undecorated silica was shown as Figure S1. Considering the decoration process would not change the formation of silica, representative N_2 sorption isotherm of OTMS decorated silica could also be illustrated by Figure S1. Because the N_2 isotherm illustrated typical type III behavior with silica, capillary condensation of VOC vapors was a major factor of adsorption behavior in the Replacing model. When silica PCs were exposed to the alcohol vapors, the replacement of reference-gas molecules with alcohol molecules occurred, forming a saddle-shaped liquid-vapor interface between two touching silica spheres, where the Replacing model was employed to explain the sensing mechanism.

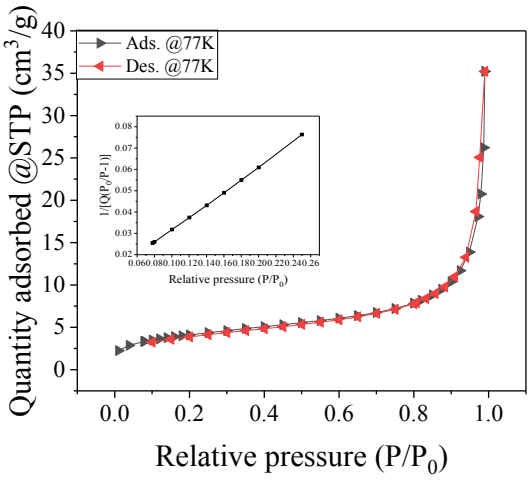

Figure S1. Representative N_2 sorption isotherm of undecorated silica.[3]

Surface area=14.6653±0.1048 m^2/g

Slope=0.294622±0.002096 g/cm^3

Intercept=0.002173±0.000326

Correlation coefficient, $\mathbf{R^2}$=0.9998230

Constant=136.563805

Pore volume=0.054097 cm^3/g

3.2 n_{OTMS} calculation.

The results of n_{OTMS} calculation was shown as Table S3. According to Sauerbrey equation (shown as Equation (1) in manuscript), Frequency shift can be easily changed into Mass shift.

$$\text{Silica weight} = (\text{Coated F} - \text{Original F})/0.0566$$

$$\text{OTMS weight} = (\text{Decorated F} - \text{Coated F})/0.0566$$

$$n_{\mathrm{OTMS}} = \text{OTMS weight}/(\text{Silica weight} + \text{OTMS weight}) \times 100\%$$

where Original F is the frequency of uncoated QCM chip when exposing to dry nitrogen. Coated F refers to the frequency of QCM chip coated with undecorated silica and OTMS decorated silica film when exposing to dry nitrogen.

So far, the content of OTMS when decoration time is 2 h, 4 h, 6 h and 8 h, respectively can be calculated as 2.62 wt%, 2.74 wt%, 3.00 wt% and 4.37 wt%.

Table S3. Original F, Coated F, Decorated F, Silica weight, OTMS weight, n_{OTMS} of undecorated silica and OTMS decorated silica.

Decoration time (h)	Original F (Hz)	Coated F (Hz)	Decorated F (Hz)	Silica weight (ng/cm^2)	OTMS weight (ng/cm^2)	n_{OTMS} (wt%)
0[3]	5002641	4939500	-	1115565.37	-	-
2	5000809	4992532	4992309	146236.75	3939.93	2.62
4	5000032	4875330	4974634	436431.10	12296.82	2.74
6	4999328	4981790	4981248	309858.66	9575.97	3.00
8	4998079	4987936	4987472	179204.85	8197.88	4.37

Chapter 4. Sensing performance and Mechanism

4.1 Sensing performance.

As the experiments ended, the computer recorded real-time Delta F dataes. According to Sauerbrey equation, Frequency shift can be easily changed into Mass shift. Figure S2 to Figure S6 illustrated the real-time Delta Mass-response curves of the QCM sensor coated with undecorated silica and OTMS decorated silica (n_{OTMS}=2.62 wt%, 2.74 wt%, 3.00 wt% and 4.37 wt%) when exposed to different atmosphere with increasing gas concentration.

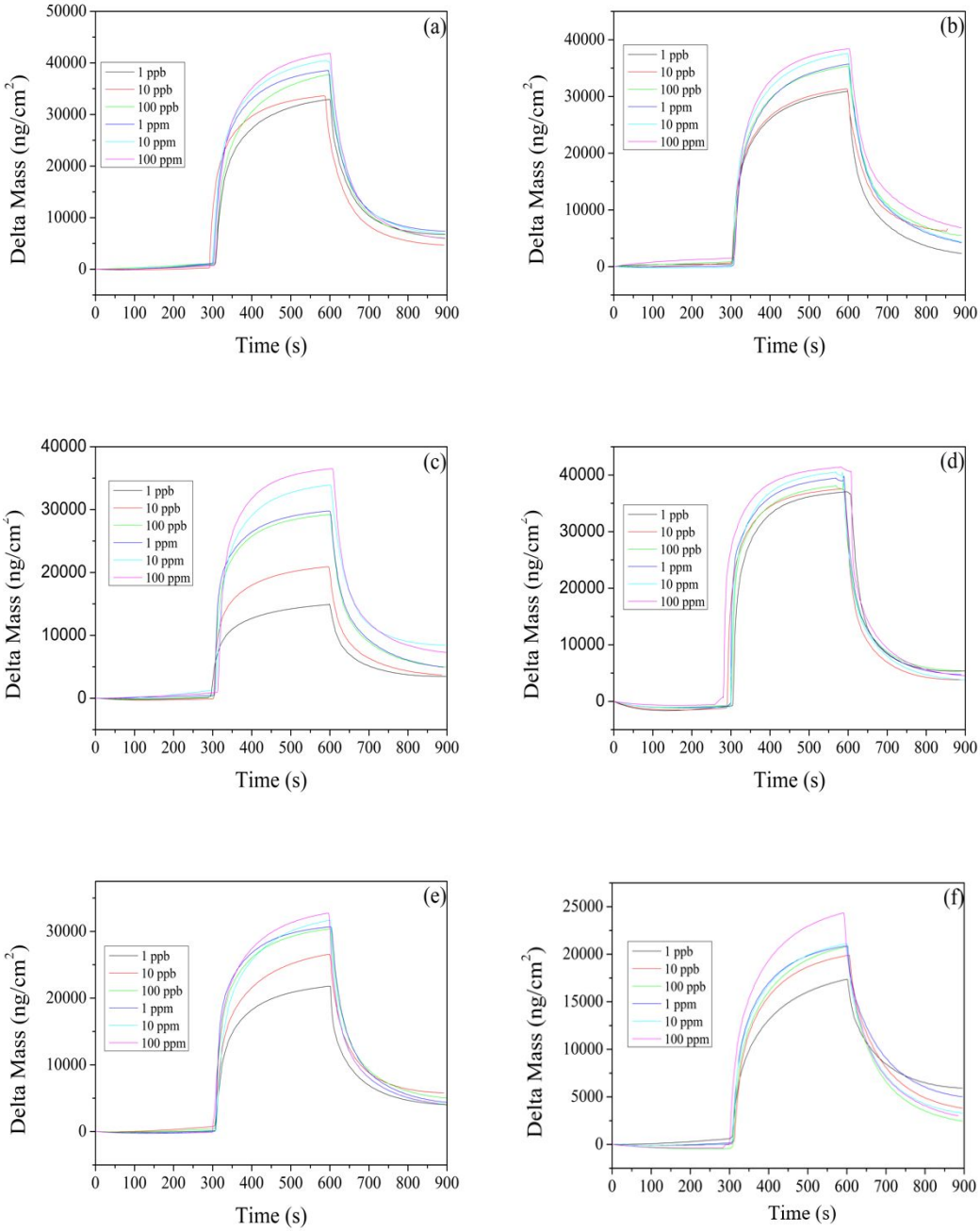

Figure S2. Real-time Delta Mass-response curves of the QCM sensor coated with undecorated silica exposed to different atmosphere with increasing gas concentration. (a) H_2. (b) O. (c) CO_2. (d) methanol. (e) ethanol and (f) isopropanol.

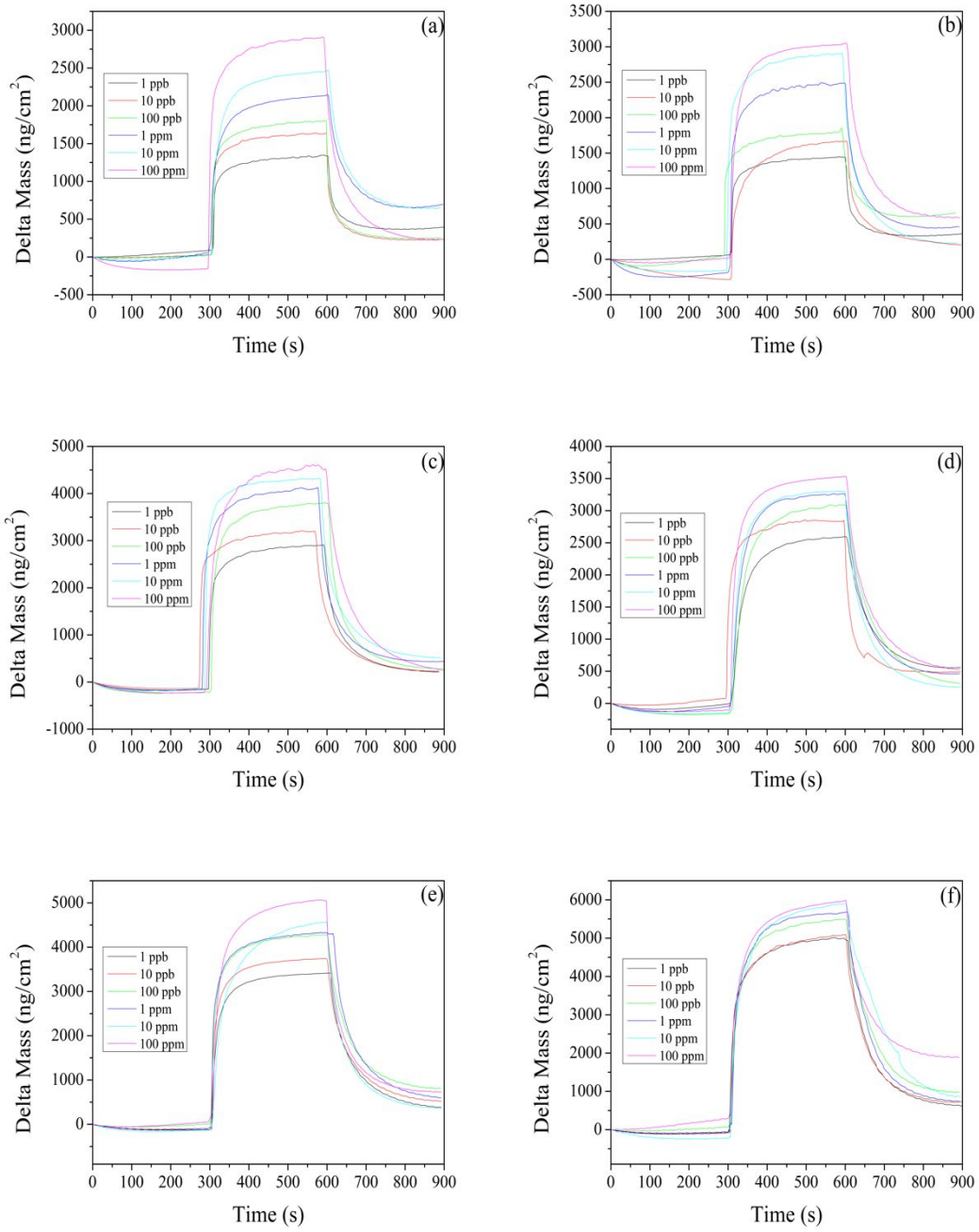

Figure S3. Real-time Delta Mass-response curves of the QCM sensor coated with OTMS decorated silica (n_{OTMS}=2.62 wt%) exposed to different atmosphere with increasing gas concentration. (a) H_2. (b) O. (c) CO_2. (d) methanol. (e) ethanol and (f) isopropanol.

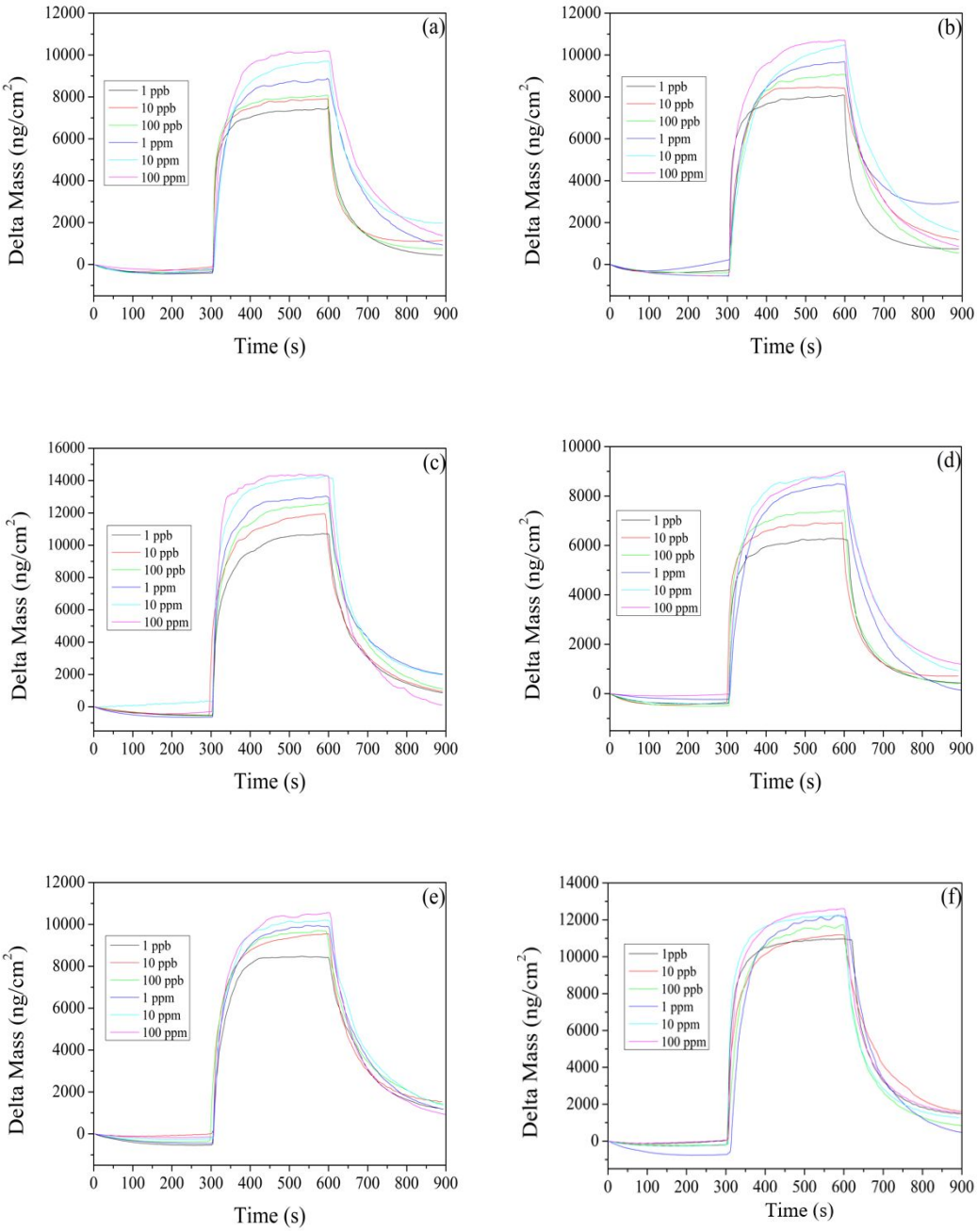

Figure S4. Real-time Delta Mass-response curves of the QCM sensor coated with OTMS decorated silica (n_{OTMS}=2.74 wt%) exposed to different atmosphere with increasing gas concentration. (a) H_2. (b) O. (c) CO_2. (d) methanol. (e) ethanol and (f) isopropanol.

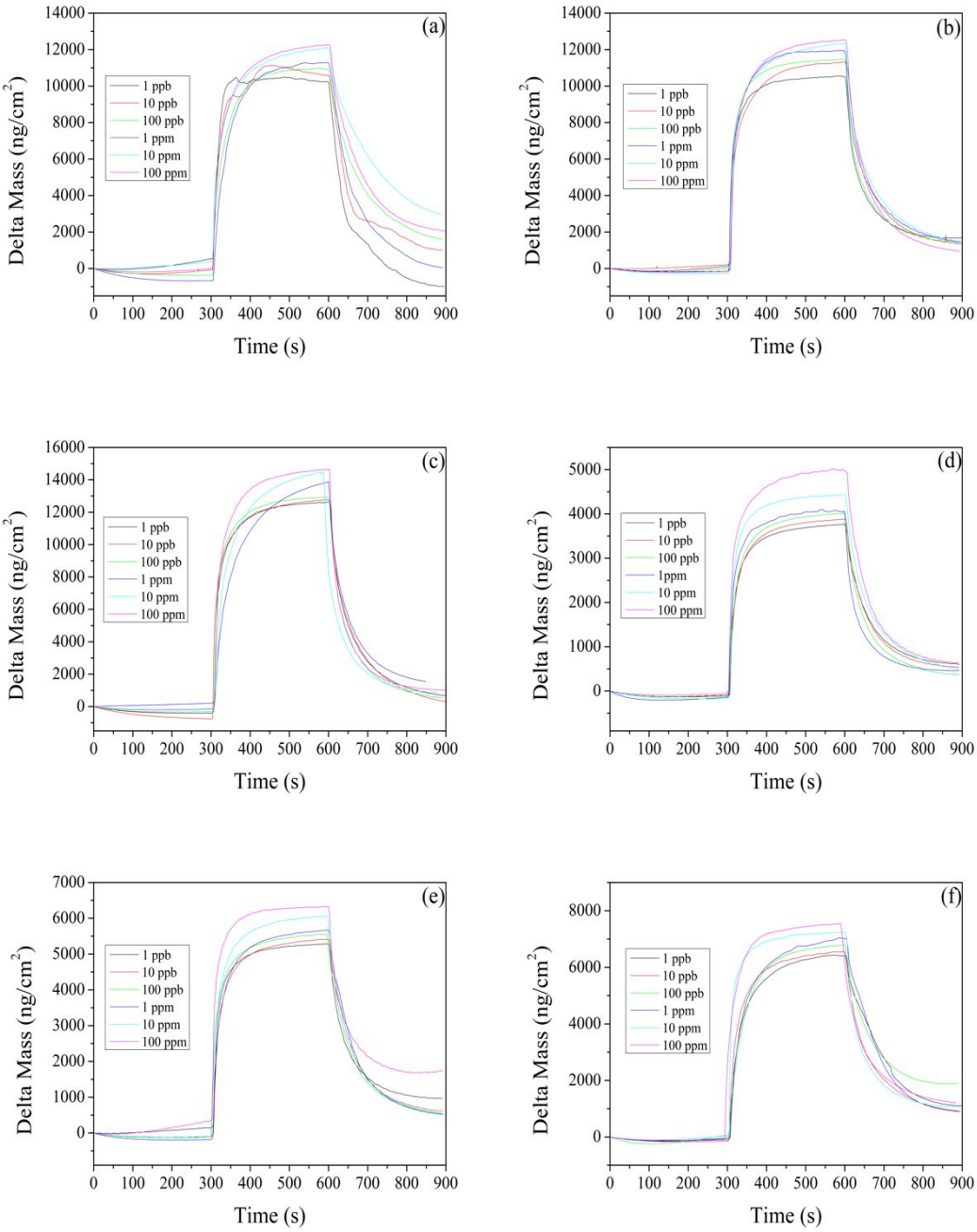

Figure S5. Real-time Delta Mass-response curves of the QCM sensor coated with OTMS decorated silica (n_{OTMS}=3.00 wt%) exposed to different atmosphere with increasing gas concentration. (a) H_2. (b) O. (c) CO_2. (d) methanol. (e) ethanol and (f) isopropanol.

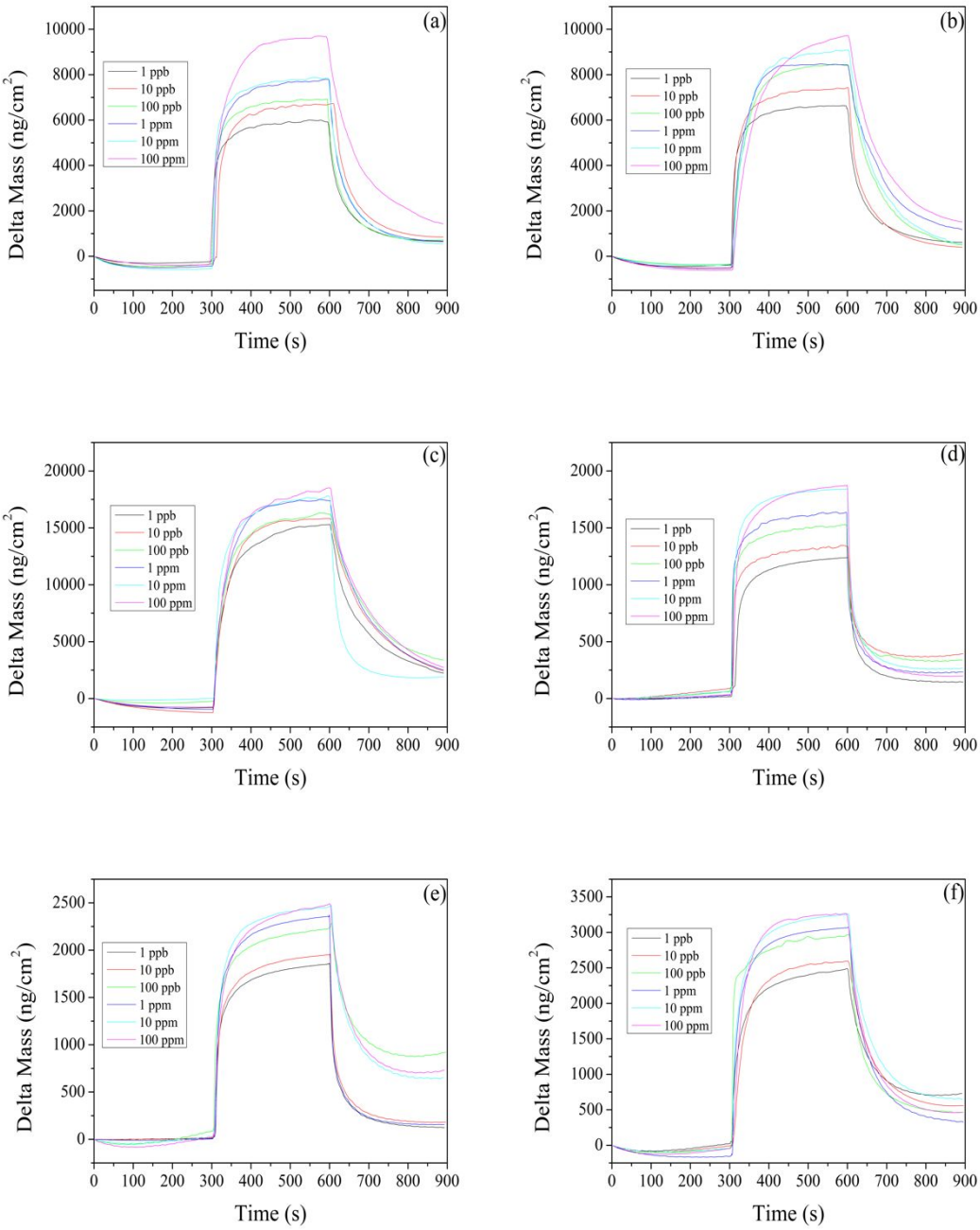

Figure S6. Real-time Delta Mass-response curves of the QCM sensor coated with OTMS decorated silica (n_{OTMS}=4.37 wt%) exposed to different atmosphere with increasing gas concentration. (a) H_2. (b) O. (c) CO_2. (d) methanol. (e) ethanol and (f) isopropanol.

4.2 Sensing Mechanism.

We have also engaged the sensing performance of other nonpolar molecule (CH_4) and polar molecules (NO and NH_3), the results were shown as Figure S7 and Figure S8, furtherly confirmed the enhancement adsorption of nonpolar molecule on modified silica was ascribed to the nonpolar group of OTMS, while the decline adsorption of polar molecule on decorated silica was caused by the nonpolar group of OTMS.

Due to the special arrangement, silica synthesized by the vertical deposition method exhibited fine selectivity among three alcohol vapors. The Replacing models were employed to explain the sensing mechanism, which had been proposed in our previous works.[3,42] The difference was that as long as the liquid-vapor interface occurred, alcohol vapors would like to entered into capillary holes of undecorated silica. As for OTMS decorated silica, alcohol vapors would like to be in connection with methyl and methylene on the OTMS molecule. $S_{\text{isopropanol,ethanol}}$ and $S_{\text{ethanol,methanol}}$ shift with increasing OTMS content under three states were shown as Figure S9a,b and the relative q shift among three alcohols were shown as Figure S9c-f, which could furtherly guide the sensing mechanism of S.

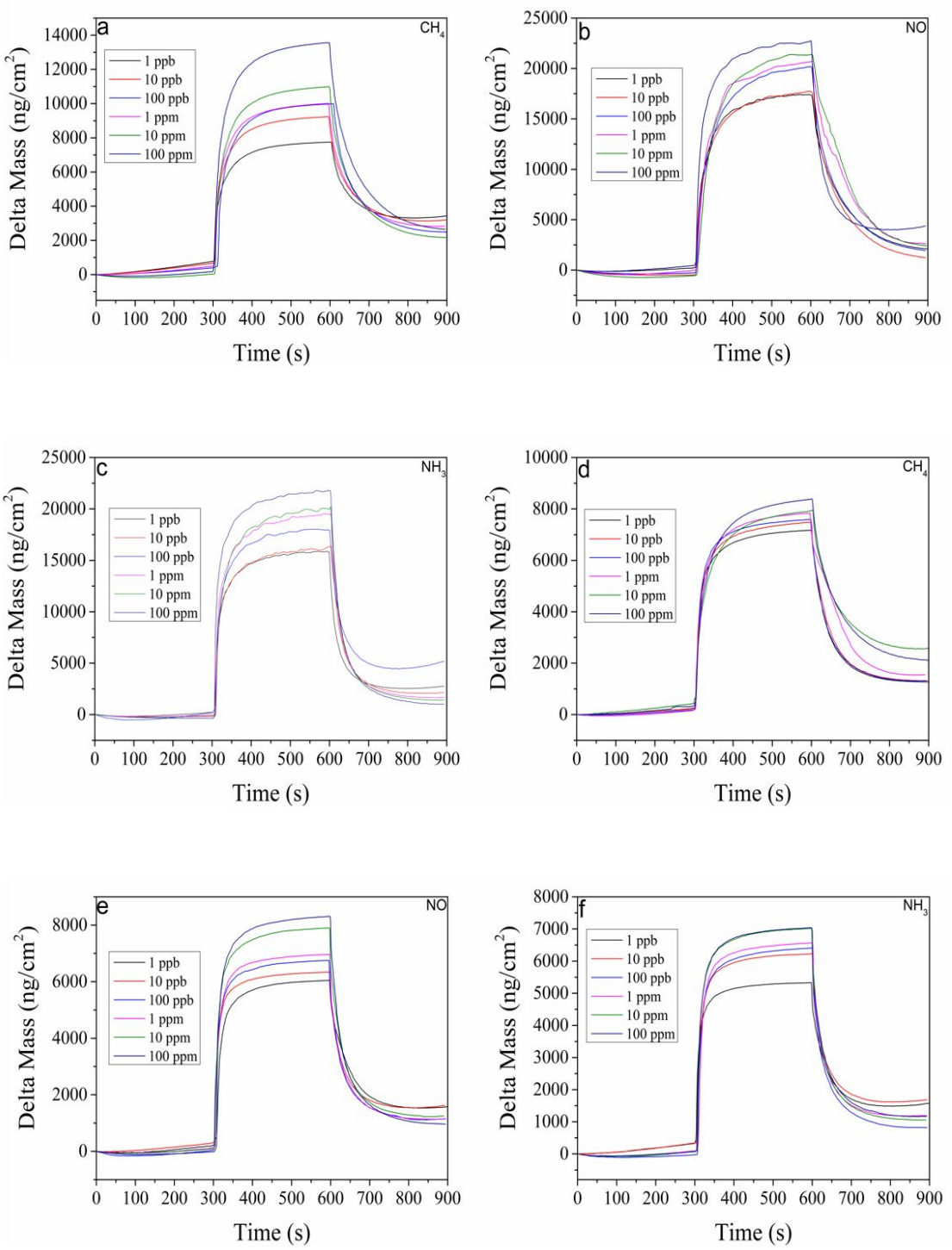

Figure S7. Real-time delta mass-response curves of the QCM sensor coated with silica exposed to three kinds of new small-molecule gases. (a) CH_4. (b) NO. (c) NH_3. Real-time delta mass-response curves of the QCM sensor coated with OTMS decorated silica (n_{OTMS}=4.37 wt%) exposed to three kinds of new small-molecule gases. (d) CH_4. (e) NO. (f) NH_3.

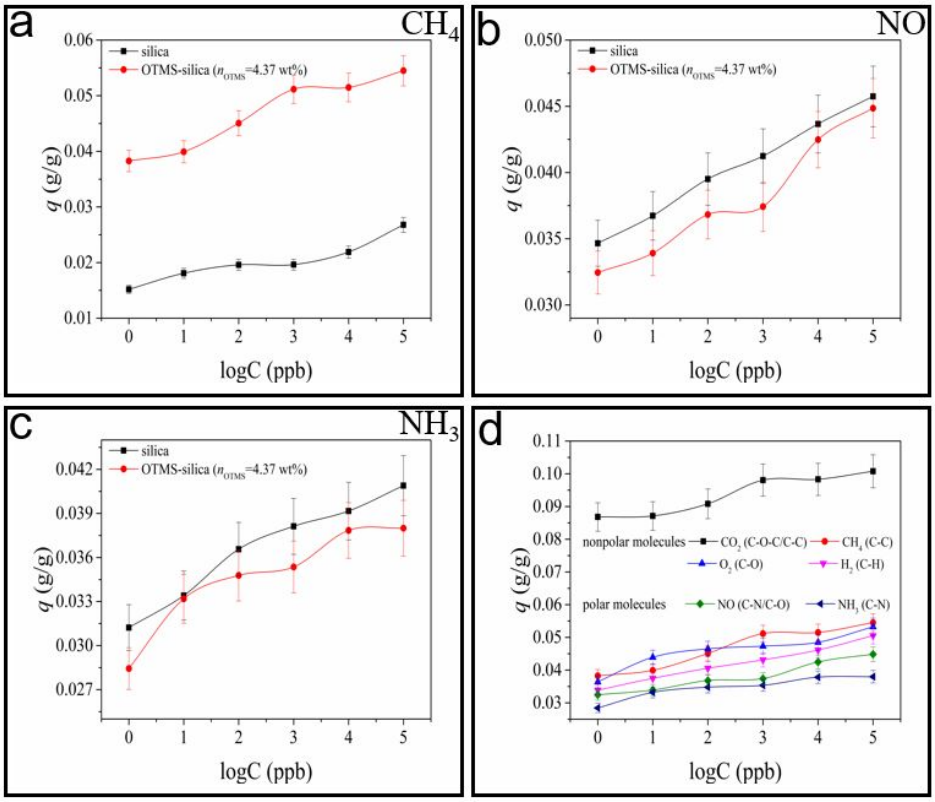

Figure S8. q~logC curves (covered error bar with ±5%) of three kinds of new small-molecule gases when QCM sensors coated with silica or OTMS decorated silica (n_{OTMS}=4.37 wt%). (a) CH_4. (b) NO. (c) NH_3. (d) comparison of q (covered error bar with ±5%) of different kinds of small-molecule gases when QCM chip coated with OTMS decorated silica (n_{OTMS}=4.37 wt%).

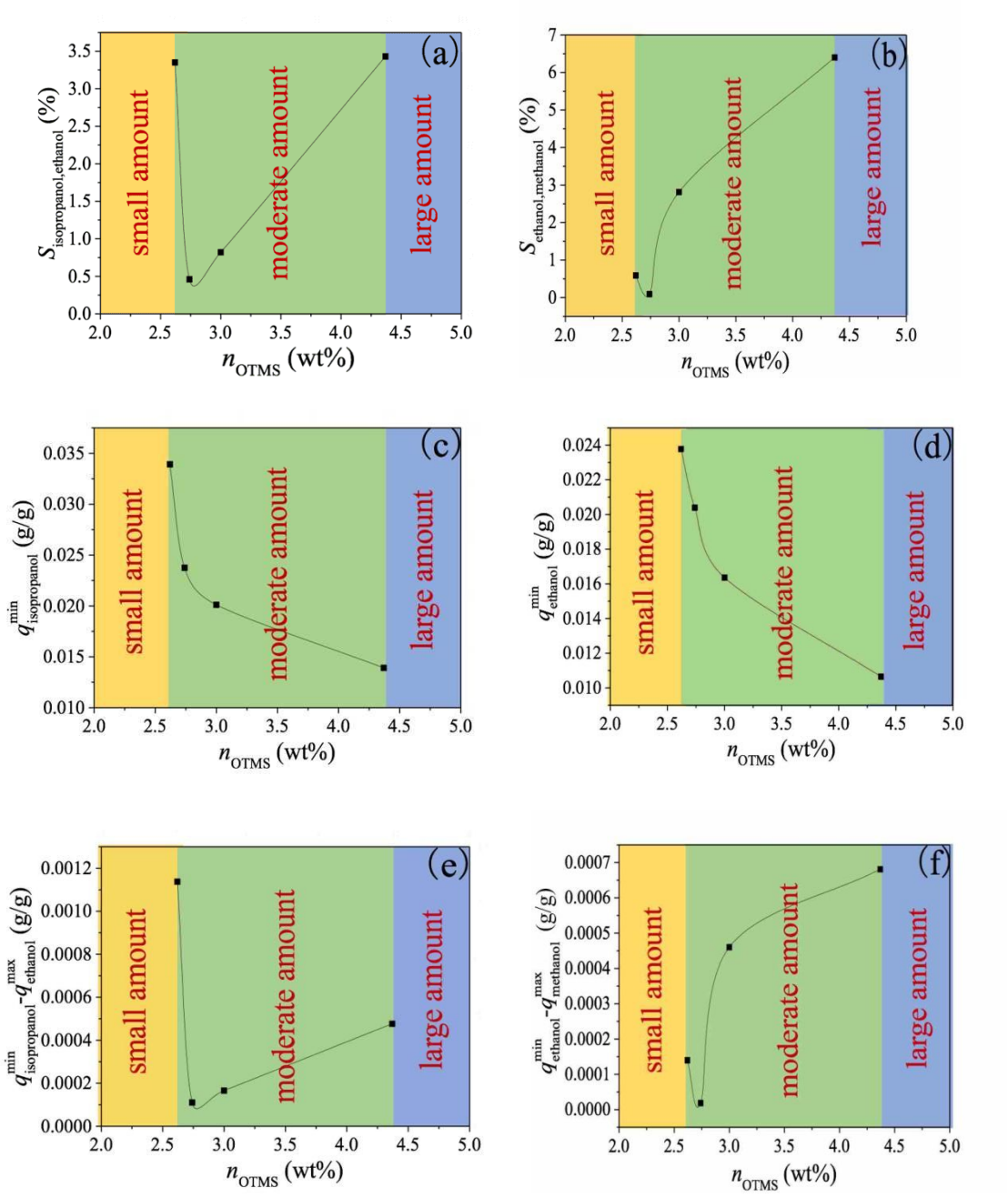

Figure S9. (a)-(b) The *S* shift when different contents of OTMS decorated silica exposed to alcohol vapors. (c)-(f) The *q* shift when different contents of OTMS decorated silica exposed to alcohol vapors.

4.3 Sensing properties of H_2O and stability

Importantly, the sensing properties of H_2O were also studied, as shown in Figure S10-Figure S12, indicating that OTMS decorated silica exhibits poor adsorption performance on H_2O. Besides, the repeatability and stability of OTMS decorated silica under different humidity and CO_2 were evaluated at room temperature (25℃), as shown in Figure S13-Figure S15, revealing fine repeatability and stability of this sensor.

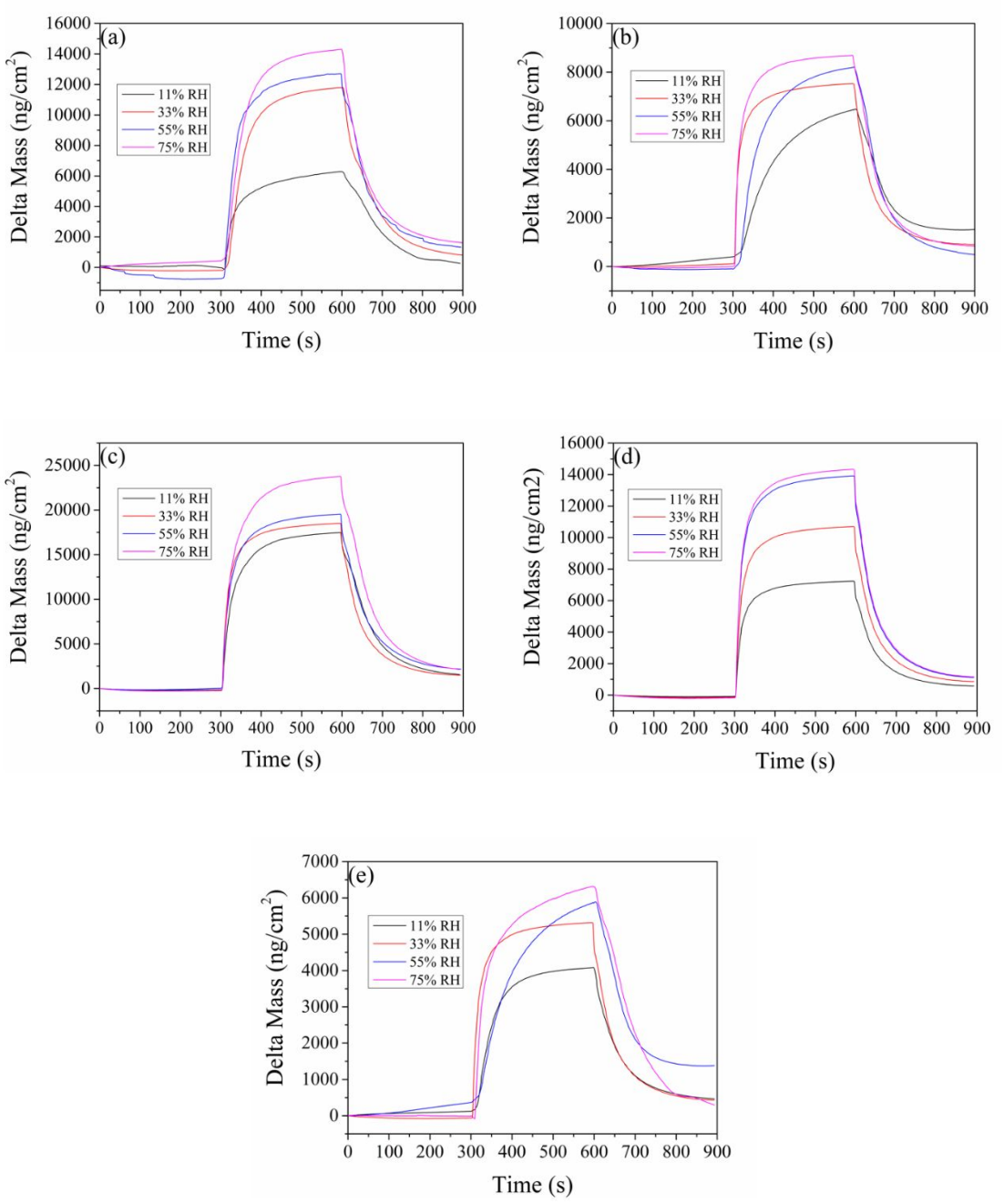

Figure S10. Real-time delta mass-response curves of the QCM sensor coated with different silica samples exposed to different relative humidity H_2O (a) undecorated silica, (b) OTMS decorated silica (n_{OTMS}=2.62 wt%), (c) OTMS decorated silica (n_{OTMS}=2.74 wt%), (d) OTMS decorated silica (n_{OTMS}=3.00 wt%), (e) OTMS decorated silica (n_{OTMS}=4.37 wt%).

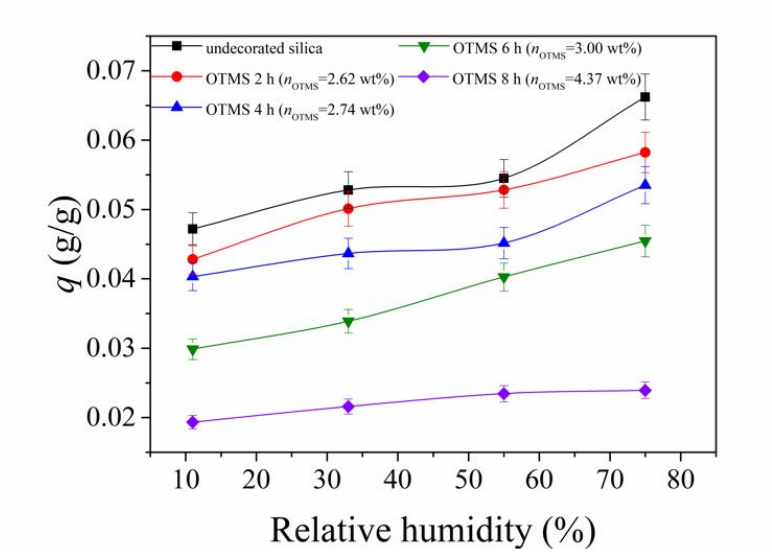

Figure S11. *q*~logC curves (covered error bar with ±5%) of different silica samples exposed to different relative humidity H_2O.

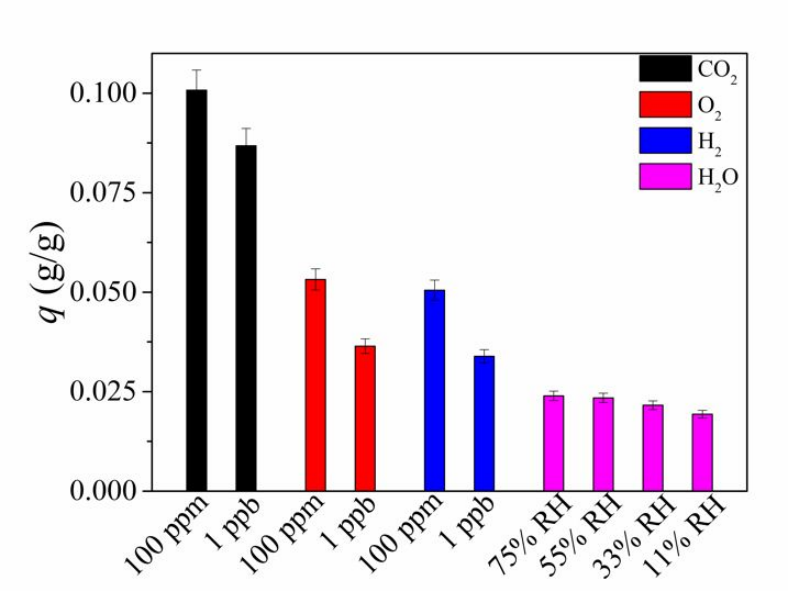

Figure S12. The comparison of q (covered error bar with ±5%) when OTMS decorated silica (n_{OTMS}=4.37 wt%) exposed to different atmosphere of different gas concentration.

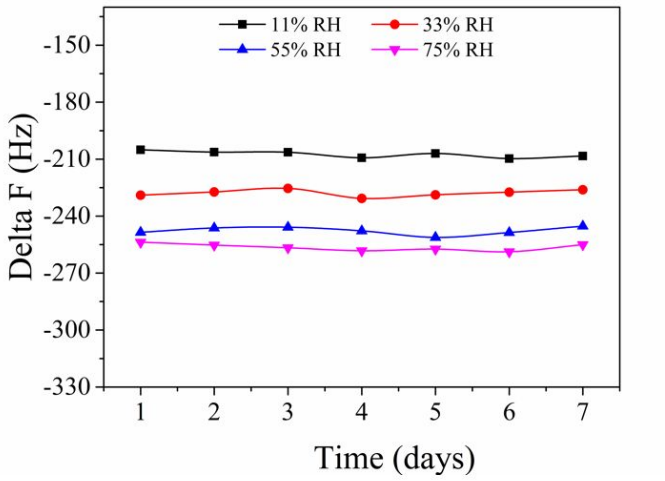

Figure S13. Stability of OTMS decorated silica (n_{OTMS}=4.37 wt%) exposed to different humidity.

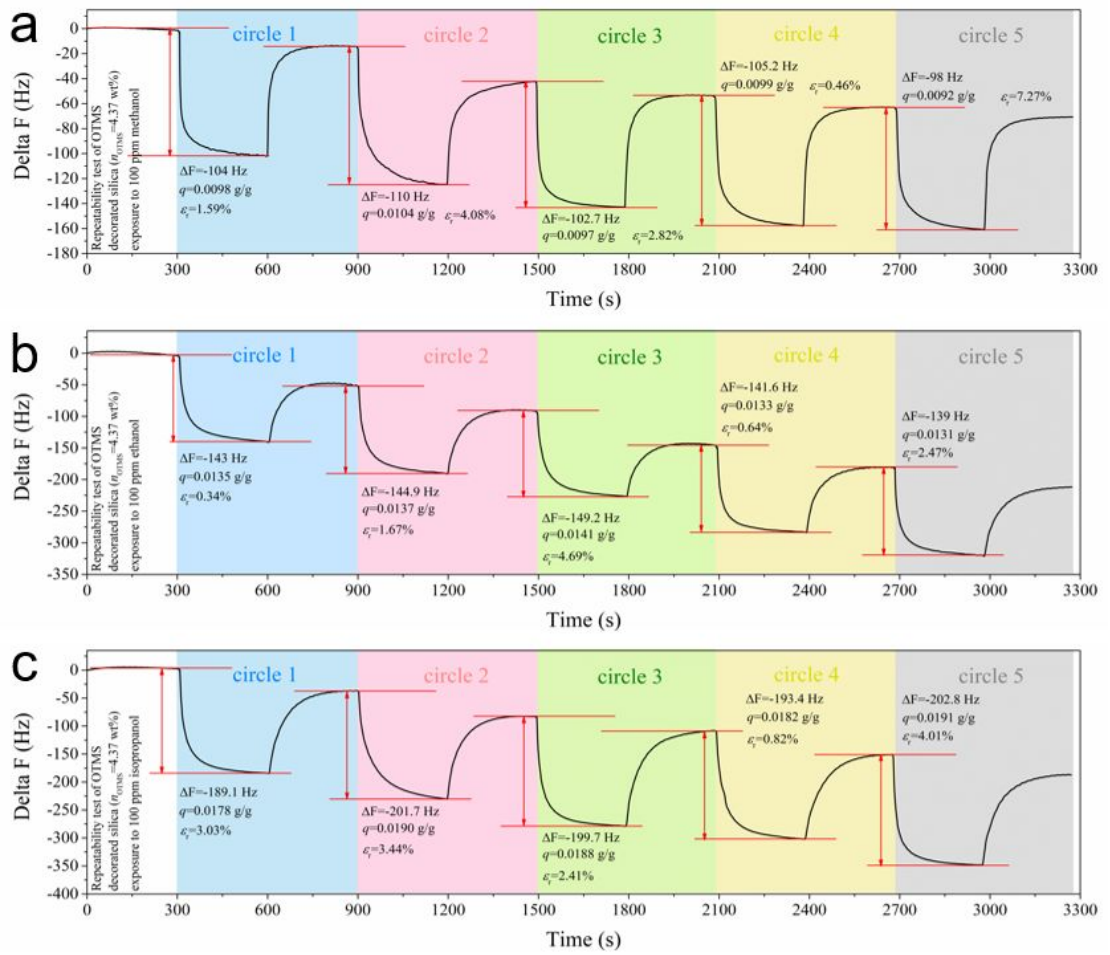

Figure S14. Repeatability of OTMS decorated silica (n_{OTMS}=4.37 wt%) when exposed to different VOCs. (a) methanol. (b) ethanol. (c) isopropanol.

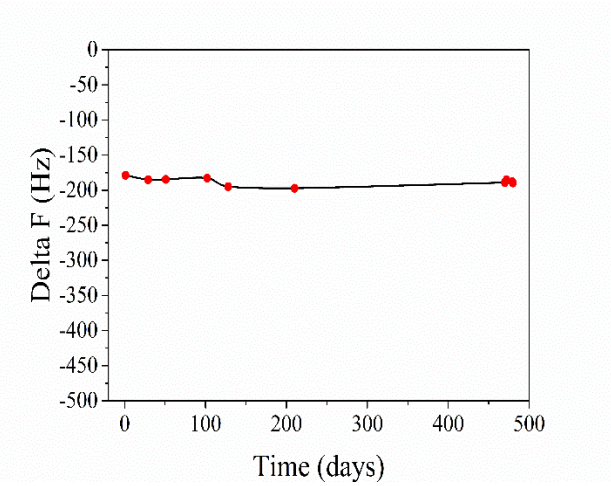

Figure S15. Stability of OTMS decorated silica (n_{OTMS}=4.37 wt%) when exposed to 100 ppm isopropanol.

4.4 Fitting and Equations.

Table S4. Equations and R^2 of CA~n_{OTMS} curve and q~CA curves.

CA (y)~n_{OTMS} (x) curve			
Equation			R^2
$y = -106301 \times e^{\frac{-x}{0.325}} + 127.19$			0.9997
q (y)~CA (x) curves			
Species	Gas concentration	Equation	R^2
H_2	1 ppb	$y = 8.47 \times 10^{-4}x - 0.071$	0.911
	10 ppb	$y = 8.60 \times 10^{-4}x - 0.070$	0.955
	100 ppb	$y = 9.31 \times 10^{-4}x - 0.076$	0.969
	1 ppm	$y = 9.10 \times 10^{-4}x - 0.072$	0.976
	10 ppm	$y = 9.37 \times 10^{-4}x - 0.073$	0.978
	100 ppm	$y = 9.81 \times 10^{-4}x - 0.075$	0.948
O_2	1 ppb	$y = 8.57 \times 10^{-4}x - 0.070$	0.950
	10 ppb	$y = 9.90 \times 10^{-4}x - 0.081$	0.994
	100 ppb	$y = 1.01 \times 10^{-3}x - 0.083$	0.989
	1 ppm	$y = 9.44 \times 10^{-4}x - 0.073$	0.965
	10 ppm	$y = 9.06 \times 10^{-4}x - 0.067$	0.962
	100 ppm	$y = 1.01 \times 10^{-3}x - 0.077$	0.953
CO_2	1 ppb	$y = 3.81 \times 10^{-8} \times e^{\frac{x}{8.827}} + 0.019$	0.999

	10 ppb	$y = 1.47 \times 10^{-8} \times e^{\frac{x}{8.304}} + 0.022$	0.998
	100 ppb	$y = 5.13 \times 10^{-10} \times e^{\frac{x}{6.814}} + 0.027$	0.999
	1 ppm	$y = 3.09 \times 10^{-10} \times e^{\frac{x}{6.603}} + 0.029$	0.999
	10 ppm	$y = 8.92 \times 10^{-10} \times e^{\frac{x}{6.992}} + 0.029$	0.999
	100 ppm	$y = 3.23 \times 10^{-10} \times e^{\frac{x}{6.617}} + 0.031$	0.999
methanol	1 ppb	$y = -3.17 \times 10^{-4}x + 0.048$	0.943
	10 ppb	$y = -3.32 \times 10^{-4}x + 0.050$	0.935
	100 ppb	$y = -4.07 \times 10^{-4}x + 0.060$	0.997
	1 ppm	$y = -4.17 \times 10^{-4}x + 0.062$	0.984
	10 ppm	$y = -4.20 \times 10^{-4}x + 0.063$	0.993
	100 ppm	$y = -4.05 \times 10^{-4}x + 0.062$	0.969
ethanol	1 ppb	$y = -3.86 \times 10^{-4}x + 0.060$	0.970
	10 ppb	$y = -4.12 \times 10^{-4}x + 0.066$	0.973
	100 ppb	$y = -4.77 \times 10^{-4}x + 0.073$	0.988
	1 ppm	$y = -5.00 \times 10^{-4}x + 0.076$	0.976
	10 ppm	$y = -5.02 \times 10^{-4}x + 0.077$	0.961
	100 ppm	$y = -5.46 \times 10^{-4}x + 0.083$	0.935
isopropanol	1 ppb	$y = -5.62 \times 10^{-4}x + 0.085$	0.916
	10 ppb	$y = -5.74 \times 10^{-4}x + 0.087$	0.961
	100 ppb	$y = -5.85 \times 10^{-4}x + 0.090$	0.958

	1 ppm	$y = -6.15 \times 10^{-4}x + 0.094$	0.934
	10 ppm	$y = -5.94 \times 10^{-4}x + 0.092$	0.921
	100 ppm	$y = -6.30 \times 10^{-4}x + 0.097$	0.883

Chapter 5. Measurements

5.1 Gas distribution process.

The high purity nitrogen (99.9999%) was used as diluent to dilute target gases, such as O_2, CO_2, and VOCs vapors. Small-molecule gases (O_2 and CO_2) with gas concentration of 1 ppb to 10^6 ppm were diluted at 25℃. Especially, the high purity argon (99.9999%) was employed to dilute hydrogen. The pure alcohol vapors (methanol, ethanol and isopropanol) were obtained from alcohols evaporation at their boiling points of 65°C, 78°C, and 82°C, respectively. Then, the nitrogen was used to dilute the alcohol vapors at the same temperature. The target VOCs gases with concentration of 1 ppb to 10^6 ppm were cooled to 25℃ before sensing measurements.

5.2 Sensing performance measurements.

As reference gas, nitrogen or argon (the target gas was hydrogen) was injected through the gas inlet and the frequency counter began to work. After the frequency signal was steady, the target gas (alcohol vapor or small-molecule gas) with concentration range from 1 ppb to 100 ppm was injected into QCM chamber and began the adsorption process. After 5 min, the reference gas was injected again. The desorption process also lasted 5 min and finished the adsorption-desorption measurement. The resonance frequencies were measured by the frequency counter and the data from QCM were recorded by computer.

5.3 Experiment environment and relative humidity test.

We have carried out the humidity response experiments at the relative humidity from 10% RH to 75% RH. According to the results (shown as Figure S16), it could not lead to large response to the change in relative humidity (from 11% to 75%). So, we thought the effect of humidity on gas sensing properties could be ignored. Furthermore, in order to keep the same measurement environment, we used a dehumidifier to maintain the environment humidity at 10% in the process of measurement.

We also carried out the gas sensing experiments when reference gases were dry nitrogen and 10 % relative humidity nitrogen. As a result (shown as Figure S17), we defined adsorption capacity (q) (shown as Equation (2) in manuscript) and relative error as follows.

$$\varepsilon_r = \frac{\left| q_{(\text{dry nitrogen})} - q_{(10\%\ \text{relative humidity nitrogen})} \right|}{q_{(\text{dry nitrogen})}} \times 100\%$$

When the dry nitrogen was used as reference gas, q is bigger than that of the reference gas of 10% RH nitrogen. But the relative error is not bigger than 5.8%. It could be explained that when the 10% RH nitrogen was employed to reference gas, some active sites on the surface of QCM may be occupied by the water molecules, resulting in decrease of q. Fortunately, the relative error was small, leading to ignore the effect of humidity on the gas sensing properties of the silica.

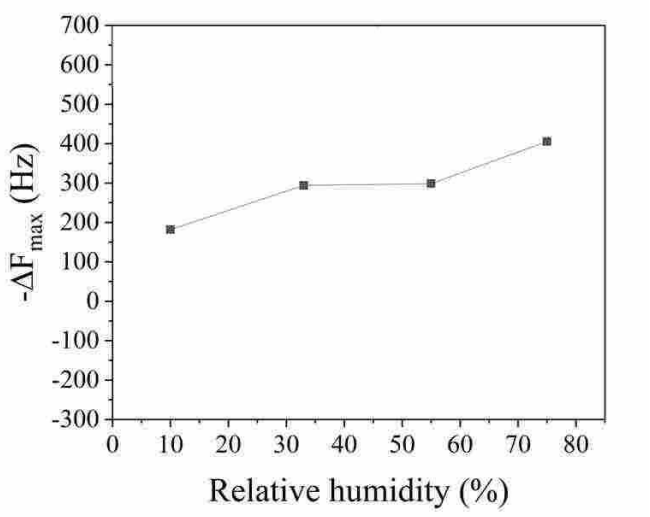

Figure S16. Comparison of -delta F_{max} of undecorated silica when QCM exposed to different relative humidity vapors.[3]

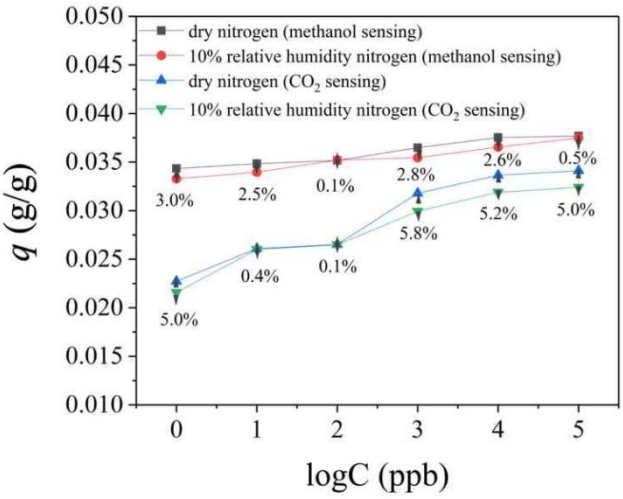

Figure S17. Comparison of adsorption capacity (q) of undecorated silica by engaging dry nitrogen or 10% relative humidity nitrogen when QCM exposed to methanol and CO_2.[3]

Reference

(1) Melde, B. J.; Johnson, B. J.; Charles, P. T. Mesoporous Silicate Materials in Sensing. *Sensors* **2008**, *8*, 5202-5228.

(2) Amonette, J. E.; Matyas, J. Functionalized Silica Aerogels for Gas-Phase Purification, Sensing, and Catalysis: A Review. *Microporous Mesoporous Mater*. **2017**, *250*, 100-119.

(3) Xie, J.; Zhang, L.; Xing, H. Y.; Bai, P. H.; Liu, B.; Wang, C. J.; Lei, K.; Wang, H.; Peng, S.; Yang, S. Gas Sensing of Ordered and Disordered Structure SiO_2 and Their Adsorption Behavior Based on Quartz Crystal Microbalance. *Sens. Actuators B* **2020**, *305*, 127479.

(4) Jia, P. G.; Fang, G. C.; Liang, T.; Hong, Y. P.; Tan, Q. L.; Chen, X. Y.; Liu, W. Y.; Xue, C. Y.; Liu, J.; Zhang, W. D.; Xiong, J. J. Temperature-Compensated Fiber-Optic Fabry-Perot Interferometric Gas Refractive-Index Sensor Based on Hollow Silica Tube for High-Temperature Application. *Sens. Actuators B* **2017**, *244*, 226-232.

(5) Abdelghani, A.; Chovelon, J. M.; Renault, N. J.; Lacroix, M.; Gagnaire, H.; Veillas, C.; Berkova, B.; Chomat, M.; Matejec, V. Optical Fiber Sensor Coated with Porous Silica Layers for Gas and Chemical Vapour Detection. *Sens. Actuators B* **1997**, *44*, 495-498.

(6) Kulkarni, S.; Patrikar, S. Detection of Propane Gas Adsorbed in a Nanometer Layer on Silica Nanowire. *Optik* **2016**, *127*, 465-470.

(7) Zhao, H. R.; Zhang, T.; Qi, R. R.; Dai, J. X.; Liu, S.; Fei, T.; Lu, G. Y. Humidity Sensor Based on Solution Processible Microporous Silica Nanoparticles. *Sens. Actuators B* **2018**, *266*, 131-138.

(8) Wang, C.; Wu, C.; Chen, I.; Huang, Y. Humidity Sensors Based on Silica Nanoparticles Aerogel Thin Films. *Sens. Actuators B* **2005**, *107*, 402-410.

(9) Attwood, D.; Osborne, D.; Costello, B. D. L.; Ratcliffe, N.; Lam, J. Fiber Optic Oxygen Sensor for Long Term Use in Jet Fuel, Featuring Phosphorescent Dye Chemically Bonded to Functionalized Silica. *Sens. Bio-sens. Res.* **2019**, *26*, 100301.

(10) Zong, J.; Zhang, Y. S.; Zhu, Y.; Zhu, Y.; Zhao, Y.; Zhang, W. J.; Zhu, Y. H. Rapid and Highly Selective Detection of Formaldehyde in Food Using Quartz Crystal Microbalance Sensors on Biomimetic Poly-Dopamine Functionalized Hollow Mesoporous Silica Spheres. *Sens. Actuators B* **2018**, *271*, 311-320.

(11) Leventis, N.; Elder, I. A. Durable Modification of Silica Aerogel Monoliths with Fluorescent 2,7-Diazapyrenium Moieties. Sensing Oxygen Near the Speed of Open-Air Diffusion. *Chem. Mater.* **1999**, *11*, 2837-2845.

(12) Leventis, N.; Rawashdeh, A. M.; Elder, I. A.; Yang, J. H.; Dass, A.; Leventis, C.

S. Synthesis and Characterization of Ru(II) Tris(1,10-phenanthroline)-Electron Acceptor Dyads Incorporating the 4-Benzoyl-N-methylpyridinium Cation or N-Benzyl-N-methyl Viologen. Improving the Dynamic Range, Sensitivity, and Response Time of Sol-Gel-Based Optical Oxygen Sensors. *Chem. Mater.* **2004**, *16*, 1493-1506.

(13) Plata, D. L.; Briones, Y. J.; Wolfe, R. L.; Carroll, M. K.; Bakrania, S. D.; Mandel, S. G.; Anderson, A. M. Aerogel-Platform Optical Sensors for Oxygen Gas. *J. Non-Cryst. Solids* **2004**, *350*, 326-335.

(14) Boday, D. J.; Muriithi, B.; Stover, R. J.; Loy, D. A. Polyaniline Nanofiber-Silica Composite Aerogels. *J. Non-Cryst. Solids* **2012**, *358*, 1575-1580.

(15) Yildirim, A.; Budunoglu, H.; Deniz, H.; Guler, M. O.; Bayindir, M. Template-Free Synthesis of Organically Modified Silica Mesoporous Thin Films for TNT Sensing. *Appl. Mater. Interface* **2010**, *2*, 2892-2897.

(16) Wang, J. Q.; Li, Z. J.; Zhang, S.; Yan, S. N.; Cao, B. B.; Wang, Z. G.; Fu, Y. Q. Enhanced NH_3 Gas-Sensing Performance of Silica Modified CeO_2 Nanostructure Based Sensors. *Sens. Actuators B* **2018**, *255*, 862-870.

(17) Liu, Y. P.; Chen, J. C.; Li, W.; Shen, D. K.; Zhao, Y. J.; Pal, M.; Yu, H. J.; Tu, B.; Zhao, D. Y. Carbon Functionalized Mesoporous Silica-Based Gas Sensors for Indoor Volatile Organic Compounds. *J. Colloid Interface Sci.* **2016**, *477*, 54-63.

(18) Gaspera, E. D.; Buso, D.; Guglielmi, M.; Martucci, A.; Bello, V.; Mattei, G.; Post, M. L.; Cantalini, C.; Agnoli, S.; Granozzi, G.; Sadek, A. Z.; Kalantar-zadeh, K.; Wlodarski, W. Comparison Study of Conductometric, Optical and SAW Gas Sensors Based on Porous Sol-Gel Silica Films Doped with NiO and Au Nanocrystals. *Sens. Actuators B* **2010**, *143*, 567-573.

(19) Armento, P.; Casciola, M.; Pica, M.; Marmottini, F.; Palombari, R.; Ziarelli, F. Silica-Zirconium Phosphate-Phosphoric Acid Composites: Preparation, Proton Conductivity and Use in Gas Sensors. *Solid State Ionics* **2004**, *166*, 19-25.

(20) Saboor, F. H.; Khodadadi, A. A.; Mortazavi, Y.; Asgart, M. Microemulsion Synthesized Silica/ZnO Stable Core/Shell Sensors Highly Selective to Ethanol with Minimum Sensitivity to Humidity. *Sens. Actuators B* **2017**, *238*, 1070-1083.

(21) Huang, J.; Qu, W. B.; Zhu, J. L.; Liu, H.; Wen, W.; Zhang, X. H.; Wang, S. F. Electrochemiluminescent Sensor Based on $Ru(bpy)_3^{2+}$-Doped Silica Nanoprobe by Incorporating a New Co-Reactant NBD-Amine for Selective Detection of Hydrogen Sulfide. *Sens. Actuators B* **2019**, *284*, 451-455.

(22) Sebok, D.; Janovak, L.; Kovacs, D.; Sapi, A.; Dobo, D. G.; Kukovecz, A.; Konya, Z.; Dekany, I. Room Temperature Ethanol Sensor with Sub-ppm Detection Limit: Improving the Optical Response by Using Mesoporous Silica Foam. *Sens. Actuators B* **2017**, *243*, 1205-1213.

(23) Kang, J.; Kim, S. Synthesis of Quaternized Mesoporous Silica SBA-15 with

Different Alkyl Chain Lengths for Selective Nitrate Removal from Aqueous Solutions. *Microporous Mesoporous Mater.* **2020**, *295*, 109967.

(24) Jurado-Gonzalez, M.; Sullivan, A. C.; Wilson, J. R. H. Selective Oxidations of Allylic Alcohols Using Vanadyl and Cobalt (II) Alkyl Phosphonate Modified Silicas. *Tetrahedron Lett*. **2004**, *45*, 4465-4468.

(25) Al-Hashimi, M.; Fisset, E.; Sullivan, A. C.; Wilson, J. R. H. Selective Oxidation of Sulfides to Sulfoxides Using a Silica Immobilized Vanadyl Alkyl Phosphonate Catalyst. *Tetrahedron Lett.* **2006**, *47*, 8017-8019.

(26) Inumaru, K.; Nakano, T.; Yamanaka, S. Molecular Selective Adsorption of Alkylphenols and Alkylanilines from Water by Alkyl-Grafted Mesoporous Alumina: A comparative study to alkyl-grafted mesoporous silica. *Microporous Mesoporous Mater*. **2006**, *95*, 279-285.

(27) Wang, Z. K.; Zhu, Y. Y.; Chen, H. T.; Wu, H. L.; Ye, C. L. Fabrication of Three Functionalized Silica Adsorbents: Impact of Co-Immobilization of Imidazole, Phenyl and Long-Chain Alkyl Groups on Bisphenol A Adsorption From High Salt Aqueous Solutions. *J. Taiwan Inst. Chem. E.* **2018**, *86*, 120-132.

(28) Srinivasan, G.; Muller, L. Influence of Solvents on the Conformational Order of C_{18} Alkyl Modified Silica Gels. *J. Chromatogr. A* **2006**, *1110*, 102-107.

(29) Poovarodom, S.; Poovarodom, S.; Berg, J. C. Effect of Alkyl Functionalization on

Charging of Colloidal Silica in Apolar Media. *J. Colloid Interface Sci.* **2010**, *351*, 415-420.

(30) Sanchez-Milla, M.; Gomez, R.; Perez-Serrano, J.; Sanchez-Nieves, J.; Mata, F. J. D. L. Functionalization of Silica with Amine and Ammonium Alkyl Chains, Dendrons and Dendrimers: Synthesis and Antibacterial Properties. *Mat. Sci. Eng. C* **2020**, *109*, 110526.

(31) Zhang, C. Y.; Liu, Y.; Sun, Y. Biochem. Lipase Immobilized to a Short Alkyl Chain-Containing Zwitterionic Polymer Grafted on Silica Nanoparticles: Moderate Activation and Significant Increase of Thermal Stability. *Eng. J.* **2019**, *146*, 124-131.

(32) Maede, H.; Mokuno, T.; Isu, N.; Kasuga, T. Thermal Properties of Silica-Based Hybrids with Different Alkyl Chains. *Ceram. Int*. **2017**, *43*, 880-883.

(33) Ali, A.; Ali, F.; Cheong, W. J. Sedimentation Assisted Preparation of Ground Particles of Silica Monolith and Their C18 Modification Resulting in a Chromatographic Phase of Improved Separation Efficiency. *J. Chromatogr. A* **2017**, *1525*, 79-86.

(34) El-Sheikh, A. H.; Sweileh, J. A.; Al-Degs, Y. S.; Insisi, A. A.; Al-Rabady, N. Critical Evaluation and Comparison of Enrichment Efficiency of Multi-Walled Carbon Nanotubes, C18 Silica and Activated Carbon Towards Some Pesticides from Environmental Waters. *Talanta* **2008**, *74*, 1675-1680.

(35) Gwarda, R. L.; Aletanska-Kozak, M.; Matosiuk, D.; Dzido, T. H. Inversion of Type Separation System in Planar Chromatography of Peptides, Using C18 Silica-Based Adsorbents. *J. Chromatogr. A* **2016**, *1440*, 240-248.

(36) Thirumalai, M.; Kumar, S. N.; Prabhakaran, D.; Sivaraman, N.; Maheswari, M. A. Dynamically Modified C_{18} Silica Monolithic Column for the Rapid Determinations of Lead, Cadmium and Mercury Ions by Reversed-Phase High-Performance Liquid Chromatography. *J. Chromatogr. A* **2018**, *1569*, 62-69.

(37) Huang, D. N.; Wang, X. Y.; Deng, C. H.; Song, G. X.; Cheng, H. F.; Zhang, X. M. Facile Preparation of Raisin-Bread Sandwich-Structured Magnetic Graphene/Mesoporous Silica Composites with C18-Modified Pore-Walls for Efficient Enrichment of Phthalates in Environmental Water. *J. Chromatogr. A* **2014**, *1325*, 65-71.

(38) Lhuillier, J.; Martin, C.; Ressier, L.; Peyrade, J. P.; Grisolia, J.; Respaud, M. Elaboration of 1 μm Square Arrays of Octadecyltrimethoxysilane Monolayers on SiO_2/Si by Combining Chemical Vapour Deposition and Nano-Imprint Lithography. *Superlattices Microstruct*. **2004**, *36*, 227-233.

(39) Zhang, X. Y.; Wang, C. Q.; Chai, W. B.; Liu, X. Y.; Zhang, Y. M. Fabrication of Superhydrophobic Kapok Fiber Using CeO_2 and Octadecyltrimethoxysilane. *Environ. Eng. Sci.* **2016**, *35*, 696-702.

(40) Pan, H.; Wang, X. D.; Xiao, S. S.; Yu, L. G.; Zhang, Z. J. Preparation and

Characterization of TiO_2 Nanoparticles Surface-Modified by Octadecyltrimethoxysilane. *Indian J. Eng. Mater. Sci.* **2013**, *20*, 561-567.

(41) Zeng, J. B.; Liu, H. H.; Chen, J. M.; Huang, J. L.; Yu, J. F.; Wang, Y. R.; Chen, X. Octadecyltrimethoxysilane Functionalized ZnO Nanorods as a Novel Coating for Solid-Phase Microextraction with Strong Hydrophobic Surface. *Analyst* **2012**, *137*, 4295.

(42) Xie, J.; Duan, M.; Bai, P. H.; Lei, K.; Yang, C.; Liu, B.; Zhang, L.; Tang, J. L.; Wang, Y. Y.; Wang, H. Gas-Sensing Mechanism of Silica with Photonic Bandgap Shift. *Anal. Chem*. **2019**, *91*, 1133-1139.